

Synchronic scattering and geometric dephasing in microwave-induced resistance oscillations.

J. Iñarrea¹

¹*Escuela Politécnica Superior, Universidad Carlos III, Leganes, Madrid, 28911, Spain .*

We present a novel quantum transport model for microwave-induced resistance oscillations (MIRO) where we prove that the instantaneous scattering rate is directly modulated by the velocity of the driven coherent state. This interaction peaks exactly at $\omega t = 2n\pi$, where the wave packets sweep through the impurity landscape at maximum speed, breaking time-reversal symmetry to generate a net direct current. Additionally, we introduce a dephasing architecture to explain amplitude saturation: a non-linear geometric dephasing ($\exp(-A/R_c)$) triggered when the displacement amplitude A of the oscillating coherent state, approaches the cyclotron radius R_c . This perfectly captures the linear-to-sublinear power crossover at high intensities, offering a fully coherent description of non-equilibrium transport.

PACS numbers:

Introduction. The discovery of microwave-induced resistance oscillations (MIRO)^{1–3} and zero-resistance states (ZRS) in high-mobility two-dimensional electron systems (2DES) has triggered a profound re-examination of quantum transport far from equilibrium. When subjected to a perpendicular magnetic field (B) and continuous microwave radiation (MW), the magnetoresistance of the 2DES exhibits macroscopic oscillations governed by the ratio of the radiation frequency to the cyclotron frequency, ω/ω_c . At high radiation intensities, the minima of these oscillations systematically evolve, leading to

the formation of states of zero resistance (ZRS). To describe the underlying microscopic mechanism, two dominant theoretical frameworks have emerged: the inelastic model⁴, which relies on a radiation-induced non-equilibrium distribution function, and the displacement model⁵, which focuses on the spatial shift of electrons during impurity-assisted scattering events under the driving microwave field. An alternative approach is provided by the radiation-driven electron orbit model^{6–9}, in which the guiding centers of Landau states-based coherent states^{10,11} undergo a harmonic oscillations driven by the microwave field. Within this picture, the irradiated longitudinal magnetoresistance (R_{xx}) comes out from the interplay between this oscillatory motion and impurity scattering events. Despite its success in capturing key experimental features, a conceptual limitation of this model lies in the implicit assumption of a time-independent scattering rate. In such a scenario, the oscillatory motion of the guiding center averages to zero over time unless phase correlations are effectively preserved during scattering events. This has motivated critical discussions regarding the role of temporal averaging and the persistence of phase-dependent contributions in the transport response.

In this work, based on the coherent states^{12–17} approach of the radiation-driven electron orbit model¹¹, we address this issue by fully solving the scattering matrix element with irradiated coherent states. Thus, we obtain a microwave-driven modulation of the scattering probability which is no longer uniform in time, but instead inherits a periodic component from the radiation field. The instantaneous scattering rate is fundamentally modulated by the physical velocity of the driven coherent state and the interaction with the random impurity potential is maximized at $\omega t = 2n\pi$, with n being a positive integer. This corresponds precisely to the kinematic peaks where the shifting Landau orbits sweep through the crystal lattice at their maximum speed. Thus, because the scattering probability is synchronized with this velocity maximum, the time-averaged transport equations yield a non-vanishing stationary direct current, which in the end

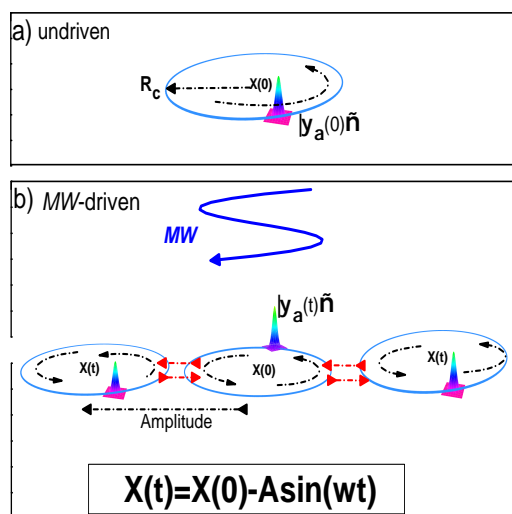


FIG. 1: Schematic diagrams of coherent states: The probability density of the coherent state is a constant-shaped Gaussian distribution, whose center oscillates in a harmonic potential similarly as its classical counterpart. The upper part exhibits the undriven or dark case. The wave packet displaces harmonically with the cyclotron frequency. The lower part exhibits the driven case, where the wave packet displaces simultaneously with cyclotron frequency, as in the upper part, and with the radiation frequency ω .

give rise to MIRO.

Furthermore, to comprehensively address the amplitude saturation observed at high microwave intensities in MIRO experiments^{18–21}, we introduce a non-linear geometric dephasing term ($\exp(-A/R_c)$), with A being the oscillation amplitude and R_c the cyclotron radius, that becomes dominant at intense driving fields and accounts for the cumulative phase friction sustained during the driven-coherent states oscillations. This geometric constraint occurs as the wave packet's spatial displacement amplitude A approaches the classical cyclotron radius, triggering a strong spatial dephasing across the impurity landscape. Thus, our model reproduces the experimental linear-to-sublinear power crossover threshold.

Importantly, the concept of a scattering rate directed by the instantaneous oscillation velocity of a driven wave packet extends far beyond the area of semiconductor heterostructures. This kinematic synchronization represents a universal feature of driven open quantum systems, sharing deep conceptual roots with the velocity-dependent dissipative dynamics observed in cold atoms in shaking optical lattices²², the time-modulated spontaneous decay of driven Rydberg states²³, and the synchronous phonon emission of oscillating solitons in Bose-Einstein condensates²⁴. By establishing that the microwave-driven 2DEG operates under these same fundamental principles, our model not only provides a clean, parameter-free resolution to the MIRO power crossover, but also establishes radiation-induced magnetotransport as a highly accessible and clean solid-state laboratory for studying universal quantum rectification.

Beyond its immediate implications for semiconductor magnetotransport, the driven coherent-state framework developed in this work establishes a profound conceptual bridge to the field of quantum computation. As an example, we can highlight that the discovered synchronization between the wave-packet's instantaneous sweeping velocity and its microscopic scattering rate provides the exact analytical counterpart to Floquet-engineered dynamical decoupling schemes, which are currently deployed to shield spin and superconducting qubits from environmental noise.

Theoretical model. According to the coherent states based extension of the microwave-driven electron orbit model, the wave function corresponding to the coherent state of the MW-driven quantum oscillator is given by^{11,25–27},

$$\psi_\alpha(x, t) \propto \phi_0[x - X(0) - x_o(t) - \langle x \rangle(t)] \quad (1)$$

where,

$$\phi_0[x - X(0) - x_o(t) - \langle x \rangle(t)] = \left(\frac{mw_c}{\pi\hbar}\right)^{1/4} e^{-\left[\frac{x - X(0) - x_o(t) - \langle x \rangle(t)}{2\Delta x}\right]^2} \quad (2)$$

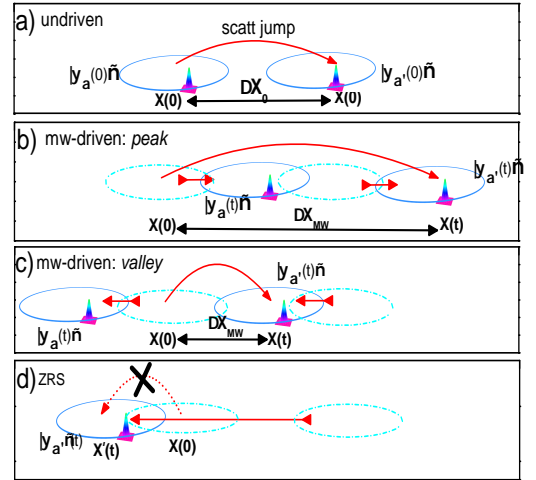


FIG. 2: Schematic diagrams for electron scattering between coherent states in the dark (undriven) and with radiation (mw-driven). a) Undriven scattering. The average distance (advanced distance) between initial $|\psi_\alpha\rangle$ and final coherent state, $|\psi_{\alpha'}\rangle$, is $\Delta X(0)$. This distance mainly determines R_{xx} . b) MW-driven scattering giving rise to peaks. Now the average advanced distance is larger because the final state, minimizing the Heisenberg uncertainty principle, is farther than the dark position due to the swinging motion of the driven-coherent states. c) MW-driven scattering giving rise to valleys. When the final coherent state is closer we obtain MIRO valleys. b) Situation when MW power is high enough and the states go backwards. In this scenario the final state ends up behind the initial state dark position and the scattering jump can not take place.

$X(0)$ is the coherent state guiding center, $\langle x \rangle(t)$ is the position mean value¹⁰, $\langle x \rangle(t) = \sqrt{\frac{2\hbar}{m^*w_c}}|\alpha_0| \cos(w_c t)$, α_0 being the coherent state amplitude¹⁰, Δx is the position uncertainty and

$$x_0(t) = \left(\frac{eE_o}{m^* \sqrt{(w_c^2 - w^2)^2 + w^2\gamma^2}} \right) \sin wt = A \sin wt \quad (3)$$

is the solution of the forced and damped classical harmonic oscillator, where E_o is the radiation electric field amplitude, γ is a damping factor for the electronic interaction with acoustic phonons, Thus, the wave function turns out to be the same as a quantum harmonic oscillator ground state where the center is driven by $x_0(t)$ and $\langle x \rangle(t)$. Then, the wave packet associated with $\Psi_\alpha(x, t)$ is therefore given by:

$$|\psi_\alpha(x, t)|^2 = |\phi_0[x - X(0) - x_o(t) - \langle x \rangle(t)]|^2 \quad (4)$$

According to the above, the microscopic physical description of a high-mobility 2DES under low or moderate B would consist of constant-shaped Gaussian wave packets

harmonically displacing with w under radiation (see Fig. 1).

To calculate the longitudinal magnetoresistance, R_{xx} , we first obtain the longitudinal conductivity σ_{xx} following a semiclassical Boltzmann model²⁸⁻³²,

$$\sigma_{xx} = 2e^2 \int_0^\infty dE \rho_i(E) (\Delta X_{MW})^2 W_I \left(-\frac{df(E)}{dE} \right) \quad (5)$$

being E the energy, $\rho_i(E)$ the Landau states density of the initial coherent state and W_I is the electron-charged impurity scattering rate. We consider now that the scattering takes place between irradiated coherent states of quantum harmonic oscillators. Thus, ΔX_{MW} is the distance between the guiding centers of the scattering-involved irradiated coherent states. According to Fermi's golden rule W_I is given by,

$$W_I = N_i \frac{2\pi}{\hbar} |\langle \psi_{\alpha'} | V_s | \psi_\alpha \rangle|^2 \delta(E_{\alpha'} - E_\alpha) \quad (6)$$

where N_i is the number of charged impurities, ψ_α and $\psi_{\alpha'}$ are the irradiated coherent states wave functions corresponding to the initial and final states respectively, V_s is the scattering potential for charged impurities²⁹: E_α and $E_{\alpha'}$ stand for the coherent states initial and final energies respectively¹⁰. The V_s matrix element is given by²⁸⁻³⁰:

$$|\langle \psi_{\alpha'} | V_s | \psi_\alpha \rangle|^2 = \sum_q |V_q|^2 |I_{\alpha, \alpha'}|^2 \quad (7)$$

where V_q is the Fourier transform of V_s and the scattering integral $I_{\alpha, \alpha'}$ ²⁸⁻³⁰,

$$I_{\alpha, \alpha'}(t) = \int_{-\infty}^{\infty} \psi_{\alpha'}(x - X'(0) - x_o(t) - \langle x' \rangle(t')) e^{iqx} \times \psi_\alpha(x - X(0) - x_o(t) - \langle x \rangle(t)) dx \quad (8)$$

where the prime indicates final scattering state.

After lengthy algebra, we obtain an expression¹¹ for $I_{\alpha, \alpha'}$,

$$|I_{\alpha, \alpha'}(t)| = e^{-\frac{[\Delta X_{MW}]^2}{8(\Delta x)^2}} e^{-\frac{q_x^2(t)2(\Delta x)^2}{4}} \quad (9)$$

where $q_x(t)$ is given by,

$$q_x(t) = q_x + \sqrt{2m\hbar w_c / \hbar} [|\alpha_0| \sin(w_c(t + \tau)) - |\alpha_0| \sin(w_c t)] \quad (10)$$

and ΔX_{MW} is given by^{11,33,34}

$$\begin{aligned} \Delta X_{MW} &= X'_{MW} - X_{MW} \\ &= \Delta X_0 - A \left(\sin w(t + \tau) - \sin wt \right) + \\ &\quad \sqrt{\frac{2\hbar}{m^* w_c}} |\alpha_0| \left(\cos w_c(t + \tau) - \cos w_c t \right) \end{aligned} \quad (11)$$

where t is the initial time for the scattering event and τ is the evolution time (flight time) between coherent states, i.e., the time it takes to reach from one state to another. An important result previously obtained in the extension of the microwave-driven electron orbit model¹¹ is that τ equals the cyclotron period T_c : $\tau = \frac{2\pi}{w_c}$.

Thus, the scattered electron begins and ends in the same position in the Landau orbit. i.e., the initial and final wave packet must occupy the same position inside the orbit at the initial and final scattering states. In other words, the quantum coherence is preserved in the scattering. Only in this case $I_{\alpha, \alpha'} \neq 0$. Thus, only scattering processes fulfilling the previous condition of τ will efficiently contribute to the current. The remaining contributions can be neglected. Thus, any event leading to decoherence during the scattering will cause the scattering fail.

Finally the expression of $I_{\alpha, \alpha'}$, after some algebra, reads²⁸,

$$|I_{\alpha, \alpha'}(t)| = e^{-\frac{q^2(\Delta x)^2}{2}} \times \left[e^{\frac{\Delta X_0 A}{2l_B^2} (\sin w(t+\tau) - \sin wt)} - \frac{A^2}{4l_B^2} (\sin w(t+\tau) - \sin wt)^2 \right] \quad (12)$$

This, in turn, leads us to a final expression for W_I ,

$$W_I = W_I(0) W_I(t) \quad (13)$$

where

$$W_I(t) = \left[e^{\frac{\Delta X_0 A}{2l_B^2} (\sin w(t+\tau) - \sin wt)} \right] \quad (14)$$

The term depending on A^2 has been neglected for moderate values of radiation intensity. The stationary (dark) term is given by¹¹,

$$W_I(0) = \frac{n_i e^4}{2\pi \hbar \epsilon^2} \int \frac{e^{-q^2(\Delta x)^2}}{(q + q_{TF})^2} (1 - \cos \theta) \delta(E_{\alpha'} - E_\alpha) d^2 q \quad (15)$$

where n_i is the charged impurity density and θ is the scattering angle. Therefore, the irradiated coherent state when under scattering gives rise naturally to an additional time-dependent factor, $W_I(t)$, that dramatically alters the dark scattering rate.

The magnetic field normally used in MIRO experiments is such that $\tau/T > 1$, T , being the radiation period. This means that during the flight time the irradiated coherent states performs many MW-driven oscillations, in which they interact with the local environment acting as a microscopic source of phase friction. This leads to decoherence or dephasing that we introduce in our model through a temporal dephasing term or decoherence factor, mathematically expressed as $\exp(-\omega\tau)$. Thus, this term accounts for the system's intrinsic loss

of quantum coherence through the radiation-driven dynamics of the coherent state during τ . Now the exponent of $W_I(t)$ is given by,

$$\frac{\Delta X_0}{2l_B^2} A e^{(-\omega\tau)} \left(\sin w(t+\tau) - \sin(wt) \right) \quad (16)$$

where we can expand the sine difference in terms of a Taylor series around wt ,

$$\begin{aligned} e^{(-\omega\tau)} \left(\sin w(t+\tau) - \sin(wt) \right) &= \\ e^{(-\omega\tau)} \left(w\tau \cos wt - \frac{w^2\tau^2}{2} \sin wt - \frac{w^3\tau^3}{3!} \cos wt + \right. \\ &\left. \frac{w^4\tau^4}{4!} \sin wt + \dots \right) \end{aligned} \quad (17)$$

Due to the aggressive asymptotic suppression driven by the exponential factor $e^{-\omega\tau}$, the higher-order terms of the series become physically redundant for large phase arguments. This ensures that the net transport modulation is mainly driven by the small- $\omega\tau$ window, fully justifying a first-order truncation where only the linear term is retained. Then, as a first approximation we can write for the sine difference,

$$e^{(-\omega\tau)} \left(\sin w(t+\tau) - \sin(wt) \right) \approx w\tau \cos wt \quad (18)$$

Substituting this result in $W_I(t)$ and Taylor-expanding the exponential we get to:

$$\begin{aligned} W_I &= W_I(0) \times \\ &\left(1 + \frac{\Delta X_0 A}{2l_B^2} w\tau \cos wt + \frac{1}{2!} \frac{\Delta X_0^2 A^2}{4l_B^4} w^2 \tau^2 \cos^2 wt \right) \end{aligned} \quad (19)$$

where we have kept only the three leading terms.

We can identify the driven coherent state's velocity ($wA \cos wt$) and this suggests that the charged impurity scattering is no longer homogeneous during the driven oscillation and takes place with more intensity where velocity is maximum. i.e., at the oscillation's midpoint, $wt = 2\pi n$. This is an important result, because our model reveals a synchronic scattering mechanism, where elastic collision rates lock dynamically to the driven coherent states. Physically, the analytical emergence of the $\cos \omega t$ dependence in the scattering rate reflects the instantaneous velocity of the driving coherent state ($v_{\text{orbit}} \propto \omega \cos \omega t$). The interaction probability is mathematically maximized at $\omega t = 2n\pi$, corresponding to the exact moments in the microwave cycle where the coherent state sweeps through space at its maximum speed. At this kinematic peak, the wave packet collides with the random impurity landscape, maximizing the scattering rate. This mechanism establishes that the

non-zero stationary current is fundamentally rooted in a velocity-dependent quantum scattering.

The next step to finally obtain σ_{xx} is to calculate the time average of the product $W_I(\Delta X_{MW})^2$, where now $(\Delta X_{MW})^2 = [\Delta X_0 - A e^{-w\tau} (\sin(wt + w\tau) - \sin(wt))]^2$. After lengthy algebra we obtain for σ_{xx} :

$$\begin{aligned} \sigma_{xx} &\propto \langle W_I(\Delta X_{MW})^2 \rangle = \\ &\left\langle \left[1 + \frac{\Delta X_0 A}{2l_B^2} w\tau \cos wt + \frac{\Delta X_0^2 A^2}{4l_B^4} w^2 \tau^2 \cos^2 wt \right] \times \right. \\ &\left. \left[\Delta X_0 - A e^{-w\tau} \left(\sin(wt + w\tau) - \sin(wt) \right) \right]^2 \right\rangle \simeq \\ &\Delta X_0^2 - \frac{2A^2 \Delta X_0^2}{4l_B^2} e^{-w\tau} w\tau \sin w\tau + \\ &\frac{A^4 \Delta X_0^2}{32l_B^4} e^{-2w\tau} w^2 \tau^2 \sin^2 w\tau \end{aligned} \quad (20)$$

The above result constitutes the core radiation part of σ_{xx} and accounts for the rise of MIRO peaks and valleys and zero resistance states (see Fig. 2). To obtain R_{xx} we use the relation $R_{xx} = \frac{\sigma_{xx}}{\sigma_{xx}^2 + \sigma_{xy}^2} \simeq \frac{\sigma_{xx}}{\sigma_{xy}^2}$, where $\sigma_{xy} \simeq \frac{n_e e}{B}$ and $\sigma_{xx} \ll \sigma_{xy}$, n_e being the 2D electron density.

In the σ_{xx} expression we observe that it depends on E_0^2 through the sine term which is the most important. This suggests a linear dependence of R_{xx} on radiation power (P). According to experimental results¹⁸⁻²¹ this happens at low P values. However, as P intensity rises the R_{xx} curve increasingly bends following a sublinear law. Above, we explained that the driven coherent state experiences decoherence along the harmonic displacement. Thus, the longer the displacement or higher P , the more intense the coherent state dephasing. To account for this effect we introduce a geometric dephasing exponential given by e^{-A/R_c} . Thus, total dephasing consists of a time-dependent part and geometric one. Consequently, the functional dependence of the photo-induced magnetoresistance amplitude ΔR_{xx} on the MW driving amplitude A is given by,

$$\Delta R_{xx} \propto A^2 e^{-(w\tau + \frac{A}{R_c})} \quad (21)$$

We can calculate the crossover from the low-power linear scaling to sublinear or the inflection point where the rate of growth changes. To determine this crossover threshold we proceed, as usual, evaluating the second derivative and setting it equal to zero. After a straightforward calculation we obtain that the crossover fulfills, $A \simeq 0.23R_c$. Accordingly, at low B , R_c is large and the crossover displaces at increasing A or P . With large values of B the crossover falls at low P values. In the former case, the curve maintains a linear behavior over a wider range of P . In the latter, the curve hardly follows a straight line and soon it bends and becomes sublinear.

Results. We first focus on the evolution of the longitudinal magnetoresistance as a function of the perpen-

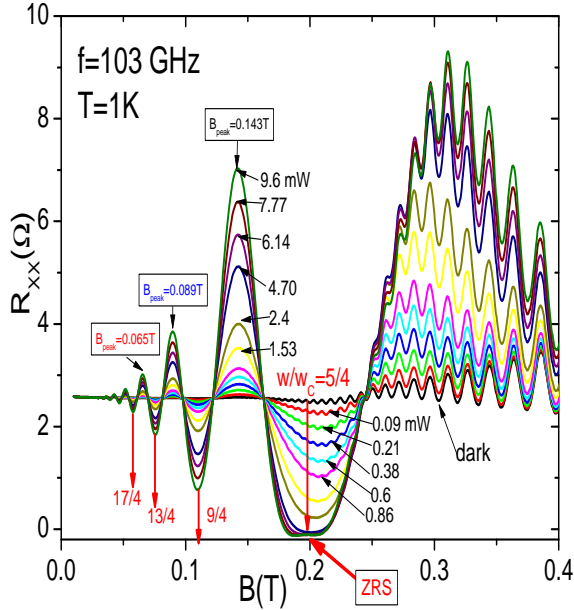


FIG. 3: Calculated magnetoresistance as a function of B , for a radiation frequency of 103 GHz and $T = 1$ K. The dark case is also exhibited. Minima positions are indicated with arrows corresponding to, $\frac{w}{w_c} = j + \frac{1}{4}$, j being a positive integer. Zero resistance states are obtained around $B \simeq 0.2T$. As the microwave power increases, the amplitude of the spatial displacement grows and ends up being reflected on the peaks and valley amplitudes.

dicular magnetic field under continuous microwave illumination. Fig. 3 illustrates irradiated and dark R_{xx} versus B curves for a fixed radiation frequency of 103 GHz and temperature $T = 1$ K at several increasing microwave power intensities. P ranges from 0.09 to 9.6 mW. As observed, the system exhibits robust resistance oscillations governed by the frequency ratio w/w_c . Our model accurately reproduces the exact positions of the resonant peaks and valleys according to experiments^{1,2}. Thus, minima positions are indicated with arrows corresponding to, $\frac{w}{w_c} = j + \frac{1}{4}$, with j being a positive integer. Zero resistance states are obtained around $B \simeq 0.2T$. This remarkable agreement stems directly from our calculation of the microscopic scattering rate using the driven coherent-state basis. Thus, we consider that the synchronicity between scattering rate and spatial oscillations of the driven coherent states is at the heart of MIRO.

As P increases, the amplitude of the driven-spatial displacement grows and ends up being reflected on the MIRO peaks and valleys. For the latter, increasing power causes MIRO valleys to collapse with the rise of ZRS. Higher power implies a larger radiation electric field, which translates into a higher coherent state displacement and a higher sweeping velocity of the wave packet

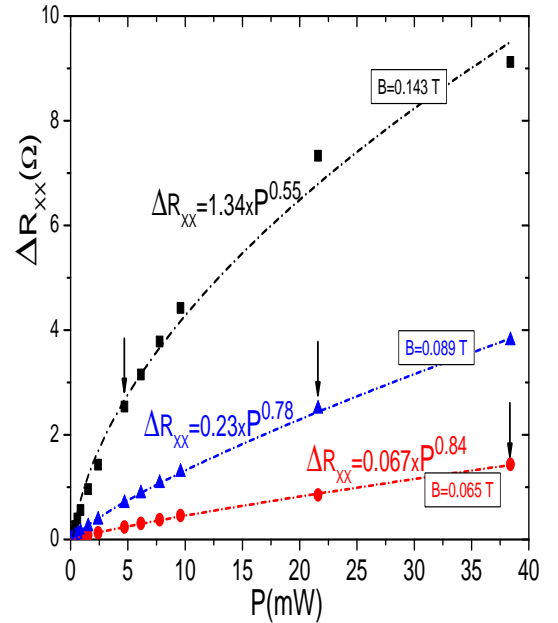


FIG. 4: Calculated amplitude $\Delta R_{xx} = R_{xx}(MW) - R_{xx}(dark)$ of the main R_{xx} peaks of Fig. 3 versus P for $f = 103$ GHz and $T = 1$ K. Also shown are the fits performed for each MIRO peak. Note that the dependence between ΔR_{xx} and P is linear first and starts to bend after the crossover point indicated by an arrow. The arrow is displaced at higher P as the peak B -value decreases. Observe that for increasing B , the exponent of the fit increases. In order to achieve a better fit we have included two extra points of higher P , 21.6 and 38.4 mW, not shown in Fig. 3.

through the crystal lattice. As explained above, the scattering probability is synchronized with the orbits MW-driven oscillations and when $wt = 2n\pi$ the orbits sweep at maximum velocity.

To unravel the microscopic constraints limiting this radiation-driven back and forth motion, we systematically analyze the non-linear power dependence of the MIRO peaks amplitude. Thus, Fig. 4 depicts the photo-induced magnetoresistance amplitude, $\Delta R_{xx} = R_{xx}(MW) - R_{xx}(dark)$, plotted as a function of the microwave power for three distinct magnetic field values: $B = 0.143$ T, $B = 0.089$ T, and $B = 0.065$ T which correspond to the positions of the three main peaks in Fig 3. The curves in Fig. 4 reveal a universal trend: at low microwave intensities, ΔR_{xx} scales strictly linearly with power, ($\Delta R_{xx} \propto P$). However, as P continues to grow, the system undergoes a crossover, entering a sublinear saturation regime.

At low fields ($B = 0.065$ T), the cyclotron radius of coherent state is large and at the same time the peak amplitude is small (see Fig. 3). Then geometric dephasing term, $e^{-(\frac{A}{\bar{r}_c})}$, remains small in the whole range of

radiation power used. Then, the irradiated magnetoresistance remains linear with P almost irrespective of the P intensity. Thus, the crossover is obtained at a higher P (see Fig. 4). As B increases, ($B = 0.089$ T) the corresponding peak is more intense, (A increases) but the cyclotron radius decreases. Thus, according to the above formula, ($A = 0.23R_c$), the ΔR_{xx} curves begin to bend and reach the crossover at smaller P . For instance, for $B = 0.143T$, ΔR_{xx} stops being linear with P very soon. Thus, the interplay of both, B and A are crucial for the coherent state dephasing. The fact that our analytical model reproduces the experimental bending¹⁸⁻²¹ confirms that MIRO saturation is not a thermal artifact, but a purely coherent, geometry-driven constraint of non-equilibrium quantum transport.

To date, while the power dependence of MIRO has been studied at specific, isolated magnetic fields¹⁸⁻²¹, a systematic experimental mapping of the linear-to-sublinear crossover as a function of the magnetic field landscape remains absent in the literature. Therefore, our dephasing framework offers a crucial, testable prediction for future magnetotransport experiments. This clear prediction provides an unprecedented opportunity for experimental verification, demonstrating that MIRO saturation is a powerful tool to probe the spatial limits of driven quantum coherence. Our model predicts a universal yet field-sensitive trend: at low microwave intensities, ΔR_{xx} scales linearly with power ($\Delta R_{xx} \propto P$), transiting into a sublinear saturation regime ($\Delta R_{xx} \propto \sqrt{P}$) at high intensities. Crucially, we predict that this crossover is highly sensitive to the magnetic field, occurring at significantly lower power thresholds as B increases (see arrows in Fig. 4).

Summary. In summary, we have developed a rigor-

ous non-equilibrium quantum transport framework for microwave-induced resistance oscillations (MIRO) based on the coherent states extension of the microwave-driven electron orbit model. We have demonstrated that the irradiated microscopic scattering rate is fundamentally dictated by the instantaneous sweeping velocity of the MW-driven coherent state. This synchronization ensures that quantum transport is mathematically driven by the kinematic peaks of the wave packet, generating a stationary direct current via an internal quantum rectification process. Furthermore, our model introduces a dual dephasing architecture that establishes a space-time duality in quantum decoherence. While high-frequency oscillations account for temporal phase dephasing, the non-linear amplitude saturation is governed by a spatial geometric dephasing term. This term naturally dictates the linear-to-sublinear power crossover as the displacement amplitude A approaches the cyclotron radius. We have shown that this geometric constraint becomes dominant at larger magnetic fields.

Ultimately, our parameter-free agreement with experimental data across different magnetic fields demonstrates that MIRO saturation is a purely coherent, geometry-driven phenomenon rather than a thermal artifact. Beyond the physics of two-dimensional electron systems, the mechanism of velocity-dependent scattering uncovered in this work aligns with universal principles of Floquet engineering and dynamic dissipation found in optical lattices and Rydberg atoms. This positions radiation-driven magnetotransport as an ideal and exceptionally clean solid-state laboratory for exploring universal quantum rectification and non-equilibrium coherent phases.

This work was supported by the MCYT (Spain) grant PID2023-149072NB-I00.

-
- ¹ R.G. Mani, J.H. Smet, K. von Klitzing, V. Narayanamurti, W.B. Johnson, V. Umansky, Zero-resistance states induced by electromagnetic wave excitation in GaAs/AlGaAs heterostructures, *Nature* **420** 646 (2002).
 - ² M.A. Zudov, R.R. Lu, N. Pfeiffer, K.W. West, Evidence for a New Dissipationless Effect in 2D Electronic Transport, *Phys. Rev. Lett.* **90** 046807 (2003).
 - ³ V. I. Ryzhii, Photoconductivity characteristics in thin films subjected to crossed electric and magnetic fields, *Sov. Phys. Solid State* **11**, 2078 (1970); V. I. Ryzhii, R. A. Suris, and B. S. Shchamkhalova, Photoconductivity of a two-dimensional electron gas in a strong magnetic field, *Sov. Phys. Semicond.* **20**, 1299 (1986).
 - ⁴ I. A. Dmitriev, M. G. Vavilov, I. L. Aleiner, A. D. Mirlin, and D. G. Polyakov, Theory of microwave-induced oscillations in the magnetoconductivity of a two-dimensional electron gas, *Phys. Rev. B* **71**, 115316 (2005).
 - ⁵ A.C. Durst, S. Sachdev, N. Read, S.M. Girvin, Radiation-Induced Magnetoresistance Oscillations in a 2D Electron Gas, *Phys. Rev. Lett.* **91** 086803 (2003).
 - ⁶ J. Iñarrea and G. Platero, Theoretical Approach to Microwave-Radiation-Induced Zero-Resistance States in

- 2D Electron Systems, *Phys. Rev. Lett.* **94** 016806, (2005).
- ⁷ J. Iñarrea, The two dimensional electron system as a nanoantenna in the microwave and terahertz bands, *Appl. Phys. Lett.*, **99**, 232115, (2011).
- ⁸ J. Iñarrea, Linear polarization sensitivity of magnetotransport in irradiated two-dimensional electron systems, *J. Appl. Phys.* **113**, 183717, (2013).
- ⁹ J. Iñarrea and G. Platero, Microwave-induced resistance oscillations and zero-resistance states in two-dimensional electron systems with two occupied subbands, *Phys. Rev. B*, **84**, 075313, (2011).
- ¹⁰ Claude Cohen-Tannoudji, Bernard Diu, and Franck Laloë, *Quantum Mechanics.* Wiley and sons. Paris.
- ¹¹ Jesus Inarrea et al. Coherent states in microwave-induced resistance oscillations and zero resistance states *Phys. Rev. Res.* **6**, 13340, (2024).
- ¹² E. Srödinger, Der stetige Übergang von der Mikro- zur Makromechanik, *Die Naturwissenschaften*, **14**, 664, (1926).
- ¹³ R.J. Glauber, Coherent and Incoherent States of the Radiation Field, *Phys. Rev.* **131**, 2766, (1963)
- ¹⁴ V.V. dodonov, ‘Nonclassical’ states in quantum optics: a ‘squeezed’ review of the first 75 years, *J. Opt. B:Quantum*

- Semiclass. Opt. **4**, R1, (2002).
- ¹⁵ B. Yurke and D. Stoler, Generating quantum mechanical superpositions of macroscopically distinguishable states via amplitude dispersion, Phys. Rev. Lett. **57** 13 (1986).
 - ¹⁶ Michael W. Noel and C.R. Stroud, Excitation of an Atomic Electron to a Coherent Superposition of Macroscopically Distinct States, Phys. Rev. Lett. **77** 1913 (1996).
 - ¹⁷ V.I. Man'ko *Theory of nonclassical states of light*. Chap. 4. Taylor and Francis. London and NewYork.
 - ¹⁸ R. G. Mani, C. Gerl, S. Schmult, W. Wegscheider, and V. Umansky, Nonlinear growth in the amplitude of radiation-induced magnetoresistance oscillations, Phys. Rev. B. **81**, 125320 (2010).
 - ¹⁹ R. G. Mani, V. Narayanamurti, K. von Klitzing, J. H. Smet, W. B. Johnson, and V. Umansky, Nonlinear growth in the amplitude of radiation-induced magnetoresistance oscillations, Phys. Rev. B. **70**, 155310 (2004).
 - ²⁰ Jesús Inarrea, R. G. Mani, and W. Wegscheider, Sublinear radiation power dependence of photoexcited resistance oscillations in two-dimensional electron systems, Phys. Rev. B. **82**, 205321 (2010).
 - ²¹ A. T. Hatke, M. Khodas, M. A. Zudov, L. N. Pfeiffer, and K. W. West, Multiphoton microwave photoresistance in a high-mobility two-dimensional electron gas, Phys. Rev. B. **84**, 241302 (2011).
 - ²² C. A. Weidner, Hoon Yu1, Ronnie Kosloff, and Dana Z. Anderson1, Atom interferometry using a shaken optical lattice, Phys. Rev. A **95**, 043624 (2017).
 - ²³ Bleuenn Bégoc, et. al, Controlled dissipation for Rydberg atom experiments, Phys. Rev. A **112**, 023312 (2025).
 - ²⁴ C. Becker, et. al. Oscillations and interactions of dark and dark-bright solitons in Bose-Einstein condensate, Nature Physics, **4**, 496 (2008).
 - ²⁵ Jesus Inarrea, Quantum superposition in ultra-high mobility 2D photo-transport, Sci Rep **16**, 5669 (2026).
 - ²⁶ E.H. Kerner, Note on the forced and damped oscillator in quantum mechanics, J. Phys. **36**, 371 (1958) .
 - ²⁷ K. Park, Radiation-induced zero-resistance state at low magnetic fields and near half-filling of the lowest Landau level, Phys. Rev. B **69** 201301(R) (2004).
 - ²⁸ B.K. Ridley. *Quantum Processes in Semiconductors*, 4th ed. Oxford University Press, (1993)
 - ²⁹ T. Ando, A. Fowler and F. Stern, Electronic properties of two-dimensional systems, Rev. Mod. Phys.**54**,(1982).
 - ³⁰ B.M. Askerov, *Electron Transport Phenomena in Semiconductors.*, World Scientific, (1994).
 - ³¹ J. H.Davies, *The physics of low-dimensional semiconductors*. Cambridge university press (1998).
 - ³² Thomas Ihn, *Semiconductors nanostructures*. Oxford University Press. New York.
 - ³³ Jesus Iñarrea, Radiation-induced resistance oscillations in 2D electron systems with strong Rashba coupling, Sci. Rep. **7**, 13573, (2017).
 - ³⁴ Jesus Iñarrea and Gloria Platero, Radiation-induced resistance oscillations in a 2D hole gas: a demonstration of a universal effect, Journal of Physics: Condens. Matter, **27** 415801 (2015).
 - ³⁵ L. Bockhorn, P. Barthold, D. Schuh, W. Wegscheider, and R.J. Haug, Magnetoresistance in a high-mobility two-dimensional electron gas, Phys. Rev. B. **83** 113301 (2011).
 - ³⁶ R. G. Mani, A. Kriisa and W. Wegscheider, Size-dependent giant-magnetoresistance in millimeter scale GaAs/AlGaAs 2D electron devices, **3** 2747 (2013).
 - ³⁷ J. Iñarrea, Theoretical model for negative giant magnetoresistance in ultrahigh-mobility 2D electron systems. EPL, **106** 47005 (2014).
 - ³⁸ M. A. Zudov, O. A. Mironov, Q. A. Ebner, P. D. Martin, Q. Shi, and D. R. Leadley, Colossal negative magnetoresistance in a two-dimensional electron gas, Phys. Rev.B, **89**, 12540, (2014).
 - ³⁹ J. Iñarrea, Photo-oscillations in MgZnO/ZnO heterostructures, Scientific Reports **12**, 22463, (2022).
 - ⁴⁰ Erwin Mönch, Denis A. Bandurin, Ivan A. Dmitriev, Isabelle Y. Phinney, Ivan Yahnuk, Takashi Taniguchi, Kenji Watanabe, Pablo Jarillo-Herrero, and Sergey D. Ganichev, Observation of Terahertz-Induced Magnetooscillations in Graphene, Nano Lett. **20**, 5943–5950, (2020).
 - ⁴¹ A. T. Hatke, M. A. Zudov, L. N. Pfeiffer and K. W. West, Giant microwave photoresistivity in high-mobility quantum Hall systems, Phys. Rev. B **83**, 121301(R) (2011).
 - ⁴² Yanhua Dai, R. R. Du, L. N. Pfeiffer and K.W. West, Observation of a Cyclotron Harmonic Spike in Microwave-Induced Resistances in Ultraclean GaAs/AlGaAs Quantum Wells, Phys. Rev. Lett. **105**, 246802 (2010).